applied sciences

MDPI

Article

Angiogenic and Osteogenic Coupling Effects of Deferoxamine-Loaded Poly(lactide-*co*-glycolide)-Poly(ethylene glycol)-Poly(lactide-*co*-glycolide) Nanoparticles

Manle Qiu [1,†], Chongyang Wang [1,†], Daoyun Chen [1,†], Chaoyong Shen [2], Huakun Zhao [1] and Yaohua He [1,*]

1 Department of Sports Medicine, Shanghai Jiao Tong University Affiliated Sixth People's Hospital, 600 Yishan Road, Shanghai 200233, China; qml198816@aliyun.com (M.Q.); doctorwangcy@163.com (C.W.); dychen1218@163.com (D.C.); zhkmssj@126.com (H.Z.)

2 Department of Gastrointestinal Surgery, West China Hospital, Sichuan University, Chengdu 610041, China; scyshenchaoyong@163.com

* Correspondence: heyaohuadoctor@163.com; Tel./Fax: +86-21-6436-9181

† These authors contributed equally to this work.

Academic Editor: Hidenori Otsuka

Received: 7 September 2016; Accepted: 29 September 2016; Published: 11 October 2016

Abstract: Angiogenesis and osteogenesis coupling processes are essential for bone regeneration, and human bone marrow stromal cells (hBMSCs) along with endothelial cells (ECs) are crucial participants. Deferoxamine (DFO), a hypoxia-mimetic agent, could activate the hypoxia-inducible factor (HIF)-1α signaling pathway and trigger angiogenic and osteogenic effects in these cells. However, the lifetime of DFO is very short, thus a suitable delivery system is urgently needed. In this study, we encapsulated DFO in Poly(lactide-*co*-glycolide)-Poly(ethylene glycol)-Poly(lactide-*co*-glycolide) (PLGA-PEG-PLGA) nanoparticles (DFO-loaded NPs) to realize its long-term angiogenic and osteogenic bioactivities. Surface morphology, size, size distribution of DFO-loaded NPs as well as DFO loading content (LC), encapsulation efficiency (EE) and release profile were systematically evaluated. When hBMSCs were exposed to the vehicle with DFO concentration of 100 μM, cells showed good viability, increased HIF-1α expression and enhanced vascular endothelial growth factor (VEGF) secretion. The transcriptional levels of the angiogenic and osteogenic genes were also upregulated. Moreover, promoted alkaline phosphatase (ALP) activity further confirmed better osteogenic differentiation. Similarly, angiogenic activity of human umbilical vein endothelial cells (HUVECs) were enhanced after the addition of DFO-loaded NPs, evidenced by increased angiogenic genes expressions and tube formation. Taken together, DFO-loaded NPs could provide a sustained supply of DFO, with its angiogenic and osteogenic coupling effects preserved, which extends the potential of this system for bone defect repair.

Keywords: PLGA-PEG-PLGA; nanoparticles; deferoxamine; drug delivery system; angiogenesis; osteogenesis

1. Introduction

Successful bone regeneration requires close coordination of various factors, such as cells, marrow stroma microenvironment and vascular networks [1]. Specifically, the neovascularization process mediated by ECs is crucial, because it not only facilitates mass exchanges, but also recruits requisite cell sources (e.g., BMSCs) for skeletal regeneration [2,3]. Besides, it is reported that osteogenic phenotype and paracrine of angiogenic factors from autologous BMSCs are also very important during bone

defect repair [4], and thus transplantation of in vitro expanded BMSCs has attracted intense interests in bone regeneration field [5]. However, a growing body of evidence has revealed that after BMSC grafting in vivo, either in the form of cell suspension or in combination with biological scaffolds, they often undergo oxygen and nutrients deprivation, which impair their survival and functionality [6,7]. This phenomenon could be mainly attributed to the impaired circulating networks in the topical damaged area of the host or the postponent neoangiogenesis in the scaffolds [1]. Therefore, the development of strategies which not only promote the osteogenic differentiation of BMSCs but also upregulate their angiogenic factors expressions to realize a rapid revascularization is urgently needed.

Reportedly, the angiogenic activities of BMSCs and HUVECs are regulated by various signaling pathways, among which the HIF-1α pathway is considered as a proximate control point [8,9]. The HIF-1α is the master regulator of oxygen homeostasis, associating with multiple physiological functions, such as glucose uptake, erythropoiesis, metabolism, cell proliferation, apoptosis regulation and angiogenesis [10]. Under normoxic conditions, HIF-1α is very unstable and easily hydroxylated by prolyl hydroxylases (PHD); while under hypoxic conditions, prolyl hydroxylation of HIF-1α is inhibited and nuclear HIF-1α accumulation occurs. The HIF-1α then heterodimerizes with the HIF-1β subunit to form an active HIF-complex and binds to the hypoxia-responsive element (HRE), which then induces transcription of multiple HIF-responsive genes, including those involved in angiogenesis, such as VEGF [11,12]. DFO, firstly used as iron chelator to treat iron overload diseases, is also a hypoxia-mimetic agent which can activate the HIF-1α signaling pathway under normoxic circumstances, and thereafter upregulate the production of various downstream angiogenesis-related factors including VEGF [11,13]. In addition, DFO can also promote osteogenic phenotype of BMSCs via the Wnt/β-Catenin signaling pathway [14,15]. Therefore, the application of DFO is expected to achieve angiogenic and osteogenic coupling effects which are essential for orthopaedics pharmacology. Nevertheless, DFO half-life is very short and it always demands repeated applications in large amounts, which is not suitable for practical use [16,17]. To tackle this shortcoming, effective local release carriers are needed.

Drug bolus, microspheres, micelles and NPs have long been studied in the domain of drug sustained release. In that regard, copolymer-based NPs are promising candidates and have been widely used because of their biocompatibility, biodegradability as well as convenient and minimally-invasive usage [18,19]. For example, recently Liao et al. prepared functionalized magnetic iron oxide/alginate core-shell nanoparticles for cancer therapy. These nanoparticles could selectively target the tumor tissue and efficiently realize a topical hyperthermia, in the existence of D-galactosamine and an AC magnetic field [20]. In another study, a macroporous scaffold derived from alginate was synthesized and showed good mineralization in cell-based bone tissue engineering applications; furthermore, hMSCs could positively attach and proliferate on this mineralized scaffold [21]. Additionally, Lin and Yeh prepared a series of alginate/hydroxyapatite (HAP) composite polymeric sponges by phase separation method. The participation of HAP into the alginate gel solution resulted in improvement of the mechanical strength and cell-attachment properties of the scaffolds [22]. According to the reported results, both of the above two studies achieved satisfying bone regeneration. Besides, compared with other vehicles, copolymer-based NPs exhibit advantages in terms of drug LC, EE, and pharmacokinetics [23]. For instance, in a study conducted by Liang et al., they encapsulated rhodamine 6G into HAP-alginate composite nanoparticles and attained an EE of approximately 63.0% [24]. Thus, in this study, we aimed to develop a NPs-based DFO delivery system that could not only realize a sustained release of DFO, but could also maintain its bioactivities over a relatively long time course. PLGA is an amphiphilic block copolymer molecule and is prone to developing polymeric NPs via self-ensemble effects. However, it has drawbacks such as excessively hydrophobicity and extremely slow degradation. Fortunately, when PLGA is PEGylation, its hydrophilicity and circulation time are improved. According to the analyses made above, we hypothesized that PLGA-PEG-PLGA NPs was a DFO delivery vehicle up to that standard. We firstly synthesized PLGA-PEG-PLGA triblock copolymers through ring-opening polymerization; next, by using the as-obtained copolymers, we prepared the PLGA-PEG-PLGA NPs with DFO encapsulated via a modified solvent extraction/evaporation method; then, we characterized

the physicochemical properties of the NPs and examined the time profile of DFO released from the NPs; last but not least, cytotoxicity of the NPs as well as the angiogenic and osteogenic coupling effects of the released DFO on hBMSCs and HUVECs were systematically studied.

2. Results

2.1. Synthesis and Characterization of Triblock Copolymer Poly(lactide-co-glycolide)-Poly(ethylene glycol)-Poly(lactide-co-glycolide) (PLGA-PEG-PLGA)

Ring-opening copolymerization between D,L-lactide (LA) and glycolide (GA) were achieved in the existence of initiator poly(ethylene glycol) (PEG) and catalyst $Sn(Oct)_2$ at 150 °C, yielding the triblock copolymers designated as PLGA-PEG-PLGA. Purified copolymers were then characterized by nuclear magnetic resonance (^{1}H NMR) in $CDCl_3$. In the spectroscopy shown in Figure 1A, peaks at 5.19 ppm and 1.56 ppm were respectively attributed to the protons (–CH–) and methyl protons ($–CH_3$) of the PLA segment. The peak at 4.82 ppm was assigned to the methylene protons ($–CH_2–$) of PGA segment, and 3.65 ppm peak represented the methylene protons ($–CH_2–$) of PEG segment [25,26]. The curve of the gel permeation chromatography (GPC) shown in Figure 1B presented a unimodal rather than a multimodal pattern, indicating the presence of successfully prepared PLGA-PEG-PLGA copolymers, not a simple physical mixture of PLA, PGA, and PEG. In addition, the molecular weight of the copolymers was determined to be 27630, which further confirmed the success of the copolymerization processes. Besides, PLGA-PEG-PLGA output was found to be about 89.5% by calculating the ratio of product weight to the theoretical value.

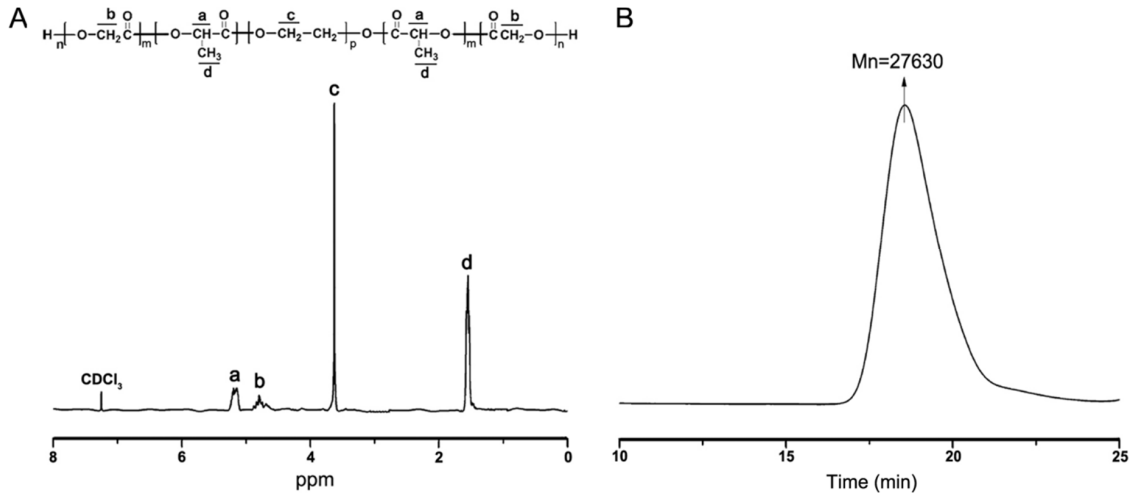

Figure 1. Nuclear magnetic resonance (^{1}H-NMR) spectra (**A**) and gel permeation chromatography (GPC) curve (**B**) of PLGA-PEG-PLGA triblock copolymers.

2.2. Preparation and Characterization of Deferoxamine (DFO)-Loaded PLGA-PEG-PLGA Nanoparticles (DFO-Loaded NPs)

By applying a solvent extraction/evaporation method, we successfully prepared the DFO-loaded PLGA-PEG-PLGA NPs (DFO-loaded NPs). Surface morphology of the DFO-loaded NPs was investigated with a field emission scanning electron microscope (FESEM), and the representative image is shown in Figure 2A. It was obvious that the DFO-loaded NPs had a spherical shape and were about 100 nm in diameter.

By using dynamic light scattering (DLS), the size of the DFO-loaded NPs was determined to be about (116.3 $\pm$ 6.5) nm in diameter, consistent with that obtained from FESEM images. Size distribution of the DFO-loaded NPs was shown in Figure 2B, displaying a narrow distribution profile. Moreover, the polydispersity index (PDI) of the NPs was less than 0.15 (mean value 0.142), further confirming

narrow size distributions of the NPs, which is a remarkable advantage for them to be efficient drug delivery vehicles. Additionally, the calculated loading content (LC) and encapsulation efficiency (EE) of DFO in the NPs were 9.8% and 98.5%, respectively. It is notable that the LC value of approximately 10% indicated a satisfactory drug loading efficiency for this system [21].

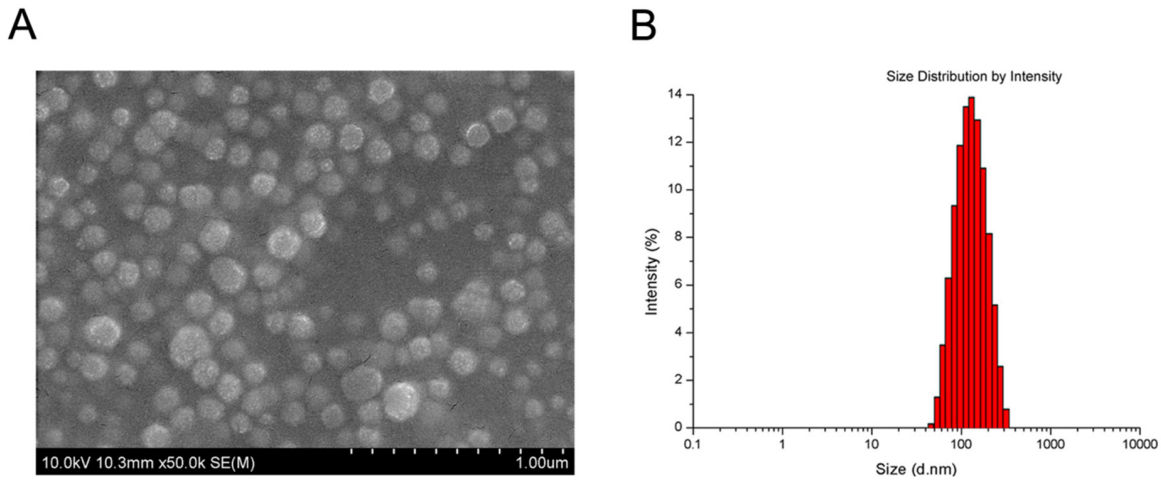

Figure 2. Field emission scanning electron microscope (FESEM) image (**A**) and dynamic light scattering (DLS) spectra (**B**) of DFO-loaded NPs.

2.3. DFO Release Profile from the PLGA-PEG-PLGA NPs

The DFO release pattern over the course of 30 days is depicted in Figure 3, showing that a total of 52.3% encapsulated DFO was released from the NPs over the first 5 days; while on day 30, it could still be detected and the cumulative release amount was 89.7%. Considering DFO half-life is very short, it is conceivable that DFO was almost completely incorporated in the NPs during preparation.

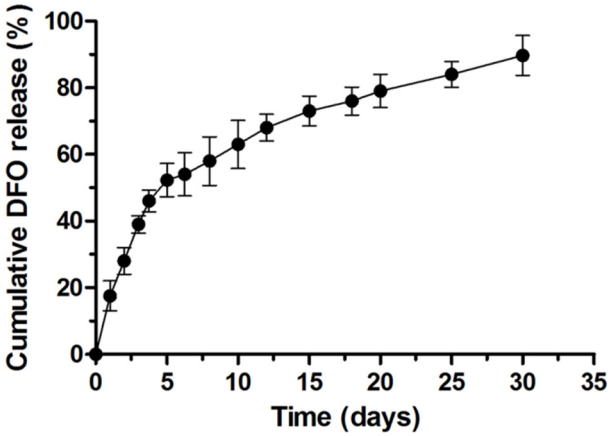

Figure 3. The in vitro DFO release profile of DFO-loaded NPs. Bars represent mean ± SD (n = 3).

2.4. The Effect of DFO-Loaded PLGA-PEG-PLGA NPs on the Viability of Human Bone Marrow Stromal Cells (hBMSCs)

To determine whether the blank or DFO-loaded NPs had any cytotoxic effect on osteogenic-involved cells, Cell Counting Kit-8 (CCK-8) and a Live/Dead cell staining assay were performed. As shown in Figure 4, hBMSCs were viable in the blank or DFO-loaded NPs groups, displaying low levels of cell death, which indicated that both the NPs and the released DFO did not have a significant effect on the viability of hBMSCs for the experiment duration of 72 h.

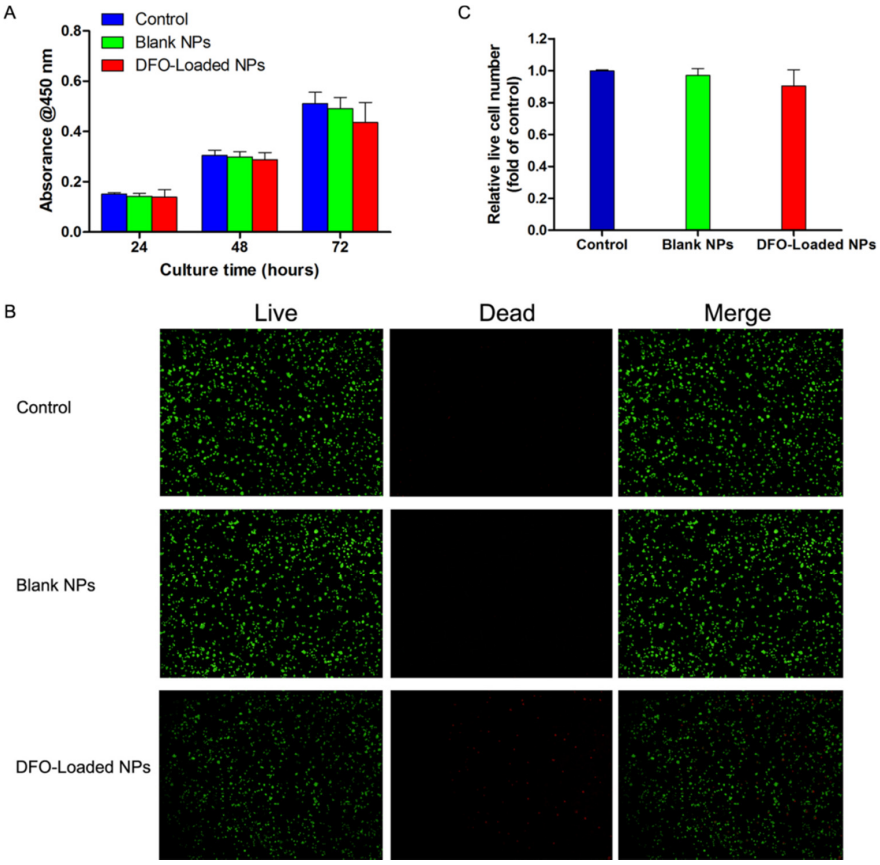

Figure 4. Cytotoxicity of the blank and DFO-loaded NPs on hBMSCs. (**A**) CCK-8 assay demonstrated acceptable cell toxicity of the NPs and the released DFO for up to 72h; (**B**) Representative images of the Live/Dead staining after cells were exposed to either NPs for 72 h. Live cells were stained green and dead cells were stained red; (**C**) Quantitation of cell death ratio in the representative images of the Live/Dead staining. Bars represent mean ± SD (n = 6).

2.5. The Angiogenic and Osteogenic Effects of DFO-Loaded PLGA-PEG-PLGA NPs on hBMSCs in Vitro

The Western blot results showed that DFO significantly enhanced HIF-1α expression of hBMSCs (Figure 5A). According to the quantitative real-time polymerase chain reaction (qRT-PCR) results, DFO-loaded NPs significantly upregulated the genetic transcription level of VEGF, the most important downstream angiogenic factor of HIF-1α pathway, in a time-dependent manner over the course of 48h (Figure 5B), while the expression levels of basic fibroblast growth factor (bFGF) and transforming growth factor (TGF)-β1 in the DFO-Loaded NPs group were similar to that of the control group or the blank NPs-treated group (Figure 5C,D). Furthermore, the ELISA results (Figure 5E–G) indicated that DFO-loaded NPs significantly promoted the protein secretion of VEGF, which has a direct stimulatory effect on angiogenesis. For bFGF and TGF-β1, although their secretions were increased in the DFO-loaded NPs group, the results had no significant difference in comparison with the other two groups, which were in accordance with the qRT-PCR results.

With regard to osteogenesis, as shown in Figure 6A, the ALP activity boosted with time in all three groups. When compared with the control group or the blank NPs group, the DFO-loaded NPs group showed significantly higher ALP activity at each predetermined time point, indicating better osteogenic differentiation. Besides, significantly enhanced osteocalcin and runt-related transcription factor-2 (Runx-2) genetic transcription levels assessed by qRT-PCR (Figure 6B,C) further demonstrated that the released DFO exerted a stimulative effect on hBMSCs osteogenic phenotype, during the experiment period.

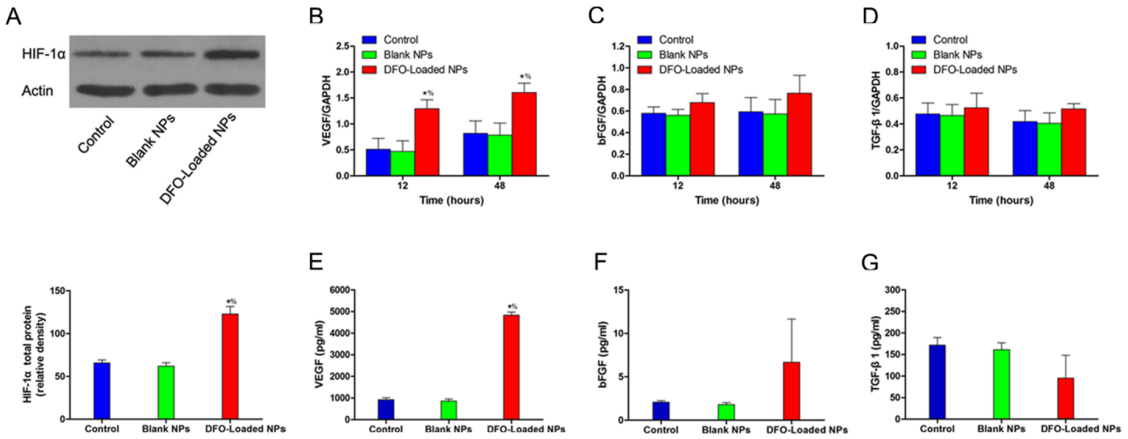

Figure 5. The angiogenic effect of DFO-loaded NPs on hBMSCs. (**A**) Representative Western blot (above) and semi-quantitative data (below) of HIF-1α expression at protein level revealed that the released DFO from NPs activated the HIF-1α signaling pathway; (**B**–**D**) Released DFO significantly increased the mRNA expression level of VEGF, both at 12 h and 48 h. While for bFGF and TGF-β1, although their transcriptional levels were upregulated in the DFO group, there was no statistical significance compared with the other two groups. Expression levels of target genes were determined by qRT-PCR, normalized using the respective expression level of glyceraldehyde-3-phosphate dehydrogenase (GAPDH); (**E**–**G**) Protein secretion levels of VEGF (**E**), bFGF (**F**) and TGF-β1 (**G**) were measured by ELISA. The VEGF protein level increased significantly after DFO treatment. For bFGF and TGF-β1, although their secretions were promoted by the released DFO, there was no significant difference due to the high variations. Bars represent mean ± SD (n = 3). * $p < 0.05$ compared to the control group; % $p < 0.05$ compared to the blank NPs group.

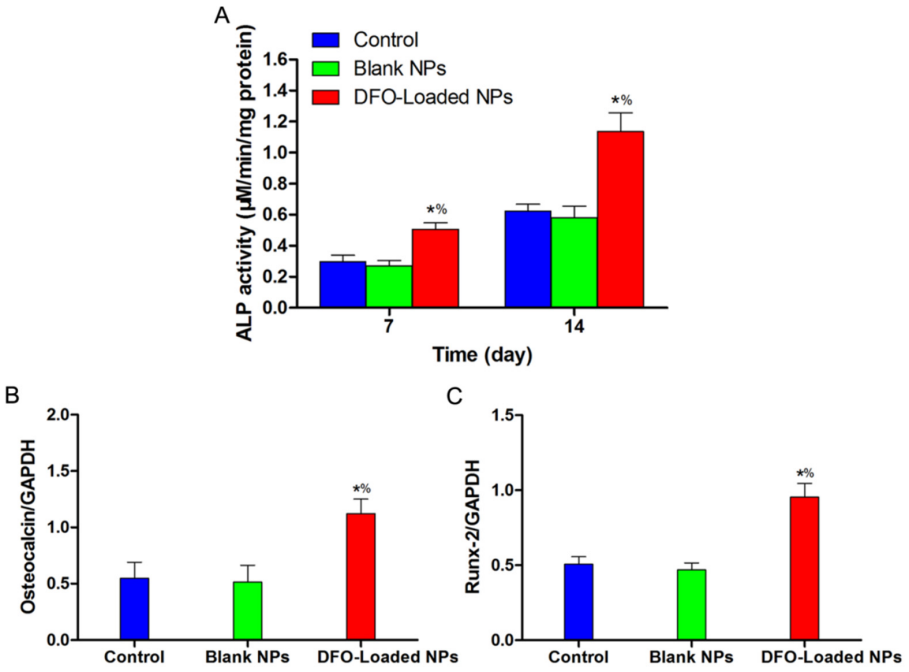

Figure 6. The osteogenic effect of DFO-loaded NPs on hBMSCs. (**A**) DFO released from the NPs significantly enhanced the ALP activity after cells were cultured in osteogenic differentiation medium for either 7 or 14 days; (**B**,**C**) The released DFO significantly increased the mRNA expression levels of osteocalcin and Runx-2, normalized using the respective expression levels of GAPDH. Bars represent mean ± SD (n = 3). * $p < 0.05$ compared to the control group; % $p < 0.05$ compared to the the blank NPs group.

2.6. The Angiogenic Effect of DFO-Loaded PLGA-PEG-PLGA NPs on HUVECs in Vitro

Considering DFO released from the NPs in situ may exert its angiogenic activity on surrounding blood vessel networks to facilitate neovascularization (endothelial cells play a vital role in this process), we employed an HUVECs monolayer + transwell plate model simulating a physiological condition to verify this hypothesis. After indirectly exposed to DFO-loaded NPs which were sequestered in the upper chamber of transwell plate, HUVECs displayed significant increment in mRNA expressions of ANGPT-2, EGF and PDGF-BB, at 24, 48 and 72 h after treatment, while for VEGF, statistical significance in the DFO-loaded NPs group existed on the latter two time points (Figure 7A–D). In addition, the tube formation analyses revealed that HUVECs contacted with the released DFO exhibited the formation of elongated and tube-like structures, whereas cells in the blank NPs group or the control group formed sparse or incomplete tubular networks, which means that DFO-loaded NPs had significantly better proangiogenic potential (Figure 7E). All these results further demonstrated that DFO-loaded NPs could remarkably enhanced the angiogenic activity of HUVECs in vitro.

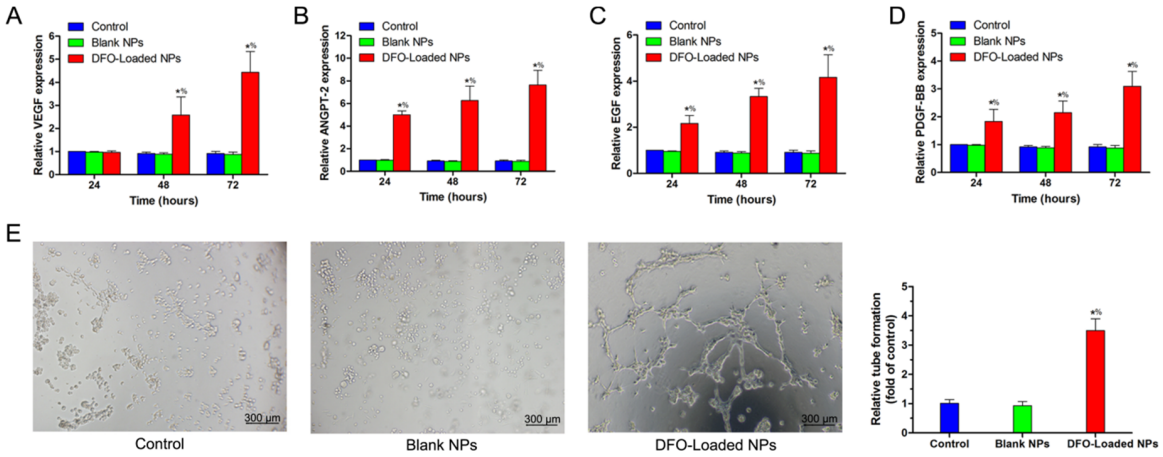

Figure 7. The angiogenic effect of DFO-loaded NPs on HUVECs. (**A**–**D**) The relative mRNA expression levels of VEGF, ANGPT-2, EGF and PDGF-BB following exposure to blank or DFO-loaded NPs solution which was sequestered in the upper chamber of transwell plate. Cells showed significantly increased genetic transcriptions for ANGPT-2, EGF and PDGF-BB at 24, 48, 72 h; for VEGF, statistical significance was found at 48 and 72 h. Bars represent mean ± SD (n = 3); (**E**) DFO released from the NPs significantly enhanced the tube formation activity after incubation for 24 h (scale bar = 300 μm). Bars represent mean ± SD (n = 5). * $p < 0.05$ compared to the control group; % $p < 0.05$ compared to the the blank NPs group.

3. Discussion

In this study, we successfully prepared PLGA-PEG-PLGA NPs from PLGA-PEG-PLGA triblock copolymers via a solvent extraction/evaporation method and demonstrated for the first time that this PLGA-PEG-PLGA NPs could support a sustained release of encapsulated DFO, with its angiogenic and osteogenic bioactivities preserved. The drug release assay showed that a total of 89.7% of the initially encapsulated DFO was released from the NPs over the duration of 30 days, in a controlled profile. Furthermore, this vehicle system showed reasonable cytotoxicity. Most importantly, we explored the pre-clinical application potential of this DFO-loaded NPs by systematically evaluating its long-term angiogenic and osteogenic coupling effects on hBMSCs and HUVECs, two most important cell types participate in human bone regeneration process.

During bone regeneration, the osteogenesis mediated by BMSCs-derived osteoblasts is of great importance [27]; on the other hand, osteogenesis is highly dependent on angiogenesis. That is to say, angiogenesis is the fundamental requirement for skeletal regeneration. The underlying mechanisms

are as follows: (1) newly formed blood vessels transport oxygen, nutrients and BMSCs that are indispensable for bone defect repair; (2) the vasculature could serve as a scaffold for bone-forming cells and new bone tissue; and (3) endothelial cells could affect bone formation indirectly via paracrine actions [2,3,28–30]. Thus, to find a therapeutic method that has the dual effects of osteogenesis and angiogenesis is a promising choice to modulate bone defect healing.

Recent studies have shown that the HIF-1α signaling pathway exerts coupling functions in physiological response mechanism, including angiogenesis and osteogenesis [31]. Iron chelators, first used in clinical practice to manage plasma iron levels, have been demonstrated to be a class of hypoxia mimics and activators of HIF-1α pathway. Accordingly, comprehensive biological and pharmacological activities were achieved by using different class of iron chelators. For example, the application of multimodal iron-chelating compounds M30 and HLA20 showed effective neuroprotective and neurorescue activities in a neural degenerative disease model [32]. Similarly, Xiao et al. reported that M30 showed a protective effect for hepatocytes against ethanol-induced injury [33]. VAR10303, another multitarget iron chelator, could improve the motor performance and extended survival rate of amyotrophic lateral sclerosis mouse when co-applied with high calorie/energy-supplemented diet [34]. While after treating pulp cells with iron chelator hinokitiol, the collected conditioned medium showed enhanced angiogenic properties both in vitro and in vivo [35]. However, as far as we know, there are few reports investigating the biological effects of DFO on hBMSCs and HUVECs, cell types that are crucial for bone regeneration. Thus, we hypothesized in this study that the application of DFO, which could activate the HIF-1α signaling pathway under normoxia conditions, would induce angiogenic factor secretions and osteogenic differentiation of BMSCs, and finally boost bone modeling. However, the lifetime of DFO is always very short, and it is necessary to exploit a local sustained release depot for it.

As aforementioned in this article, NPs are considered to be superior drug delivery vehicles. Specially, amphiphilic block copolymers are naturally inclined to form self-assembled NPs through hydrophobic-lipophilic interactions [25]. PLGA is a widely used biomedical material, but it has weak hydrophilicity and degrades too slowly to meet the needs of drug delivery, and PLGA NPs would be easily removed by the mononuclear phagocytic system (MPS) [36]. By introducing PEG into a PLGA framework, we solved these problems and successfully prepared the desirable PLGA-PEG-PLGA NPs, with efficient DFO encapsulation. Besides, as shown in Figure 3, this NPs vehicle system provided favorable sustained release for DFO.

However, a growing body of evidence has revealed that DFO is prone to inactivation. Consequently, to push ahead the application range of this DFO-loaded NPs, the key point is to verify that the encapsulated DFO indeed stays pharmacologically active in a long time course. Hence, in this study, we systematically evaluated the in vitro bioactivities of the controlled released DFO. For hBMSCs, they survived and proliferated well in the DFO-loaded NPs formulation (Figure 4), and the western blot assay indicated that the HIF-1α expression level was significantly upregulated in the DFO group compared with the blank NPs group or the control group (Figure 5A). By applying qRT-PCR, we observed that the DFO group showed a significantly higher genetic transcription level of VEGF-one of the most important HIF-1α target genes for angiogenesis-although other monitored genes such as bFGF and TGF-β1 remained unchanged (Figure 5B–D); similarly, the osteogenic genes including osteocalcin and Runx-2 exhibited significant upregulation (Figure 6B,C). Additionally, the ELISA results confirmed a significantly increased VEGF expression, despite not for bFGF or TGF-β1, in protein level (Figure 5E–G); and the ALP activity assessment further revealed that the DFO-loaded NPs continuously enhanced osteogenic differentiation of hBMSCs for the duration of the experiment (Figure 6A).

For HUVECs, as shown in Figure 7, DFO-loaded NPs significantly enhanced their angiogenic activity for up to 72 h, which was evidenced by promoted genetic transcription levels of VEGF, ANGPT-2, EGF and PDGF-BB, as well as the bolstered tube formation. Notably, the effect of DFO-loaded NPs on the HUVEC monolayer below resembled the natural paracrine model since HUVECs and the NPs were deliberately segregated using the transwell plate. According to the analyses

made above, DFO-loaded NPs have the potential to be an in situ depot for the sustained release of DFO and provide strong angiogenic and osteogenic coupling stimuli for bone regeneration applications.

To conclude, this study demonstrated that the PLGA-PEG-PLGA NPs prepared from a modified solvent extraction/evaporation method possessed favorable biocompatibility and could be used as DFO nanocarriers, with a sustained release profile and the in vitro angiogenic and osteogenic properties well preserved in a fairly long time course. However, further in-depth study of the material and in vivo investigations are needed to advance the application of this drug delivery system in the field of bone regeneration.

4. Materials and Methods

4.1. Materials

LA, GA, PEG, stannous octoate ($Sn(Oct)_2$) and DFO were purchased from Sigma-Aldrich (St. Louis, MO, USA). Acetonitrile and methanol were purchased from EM Science (HPLC grade, Mallinckrodt Baker, Phillipsburg, NJ, USA). All other solvents and chemicals in reagent grade were purchased from GuoYao Regents Company (Shanghai, China), except where otherwise indicated, and used as received.

4.2. Synthesis and Characterization of PLGA-PEG-PLGA Copolymers

PLGA-PEG-PLGA triblock copolymers were synthesized from LA, GA, and PEG with catalyst $Sn(Oct)_2$ by ring-opening copolymerization. In brief, calculated amounts of monomers LA, GA, initiator PEG, and $Sn(Oct)_2$ as the catalyzer were added in a glass tube under vacuum. And a nitrogen filling-exhausting process was repeated for 3 times to remove air and moisture residues from the reactants. The reaction was carried out at 150 °C in oil bath for 12 h with argon protection. Afterwards, the tube was cooled at room temperature, and the as-obtained products were dissolved in dichloromethane, precipitated in large amounts of cold methanol and filtered for purification. The final PLGA-PEG-PLGA triblock copolymers were collected after vacuum-dried at 40 °C for 2 days. ^{1}H NMR (Varian 400 spectrometer, Santa Clara, CA, USA) spectra was conducted to characterize the chemical structure of the copolymers by dissolving samples in $CDCl_3$. To determine the molecular weight as well as molecular weight distribution of the copolymers, we used GPC (Agilent 110 HPLC, Palo Alto, CA, USA) at a flow rate of 1 mL/min, with tetrahydrofuran (THF) as the eluent. Molecular weights were calibrated according to standard polystyrene samples.

4.3. Preparation of DFO-Loaded PLGA-PEG-PLGA NPs

DFO-loaded NPs were prepared by a solvent extraction/evaporation method, according to a previous report [37] but with some improvements. Briefly, 5 mg of DFO and 100 mg of the copolymers were dissolved in 8 mL of dichloromethane. The composite solution was then poured into 100 mL of a 1% polyvinyl alcohol (PVA) diluting in deionized water under gentle agitation. Ultrasonic emulsification was applied at an output of 25 W for 120 s to give an O/W emulsion from the mixture, and afterwards, the emulsion was evaporated overnight under reduced pressure to eliminate dichloromethane. Unencapsulated DFO and the emulsifier PVA were further removed from the resultant NPs suspension through the processes of centrifuging at 20,000 rpm for 15 min and washing with deionized water for 3 times. The final DFO-loaded NPs were freeze-dried for 2 days for the following use. Blank NPs were also prepared for comparison usage.

4.4. Characterization of DFO-Loaded PLGA-PEG-PLGA NPs

The surface morphology of DFO-loaded NPs was imaged by using an S-4800 FESEM (Hitachi, Tokyo, Japan). In short, samples of the NPs were mounted on the stub, coated with platinum, and then viewed under the FESEM at the accelerating voltage of 5.0 kV.

It has been reported that the physicochemical features of the biological NPs play an important role in the ex vivo drug release, cellular uptake and cell toxicity, as well as their in vivo actions such as pharmacokinetics and biodistribution [38,39]. Thus, we estimated the size and size distribution of the DFO-loaded NPs, two most representative parameters, by using dynamic light scattering (DLS) and Malvern Mastersizer 2000 (Malvern Instruments Ltd., Malvern, UK). Briefly, freshly-obtained DFO-loaded NPs were firstly diluted to a concentration of 1 mg/mL. After equilibration for 10 min at room temperature, measurements were carried out in triplicate to achieve the data.

Next, we determined the DFO LC and EE of the NPs using high-performance liquid chromatography (HPLC, LC 1200, Agilent Technologies, Santa Clara, CA, USA) as previously reported [21]. In brief, 5 mg of DFO-loaded NPs were completely homogenized in 1 mL of dichloromethane under vortex oscillation, then the solution was transferred to 5 mL of mobile phase containing the same volume of deionized water and acetonitrile. After evaporating the dichloromethane residues via a nitrogen stream perfusion method, a clear solution suitable for HPLC analysis was prepared. HPLC analysis was performed by using a reverse-phase C18 column (150 mm × 4.6 mm, 5 μm, C18, Agilent Technologies, Palo Alto, CA, USA) with the set flow rate of mobile phase as 1 mL/min. The column effluent was assessed by applying a UV detector at λ_{max} of 227 nm. Drug LC is calculated as the ratio of incorporated DFO amount to the weight of NPs, while drug EE was defined as the mass of DFO encapsulated in the NPs divided by that of DFO fed in the synthesizing process [40].

4.5. In Vitro DFO Release Assay

Solutions of DFO-loaded NPs were prepared with DFO at a 100 μM concentration. We chose this concentration since 100 μM of DFO could effectively activate HIF-1α signaling pathway and promote the expression of its downstream genes, for in vitro-expanded hBMSCs and HUVECs [10,41,42]. Based on this consideration, DFO concentrations in the following solutions were all set as 100 μM. According to a previous paper [43], we used dialysis method for this in vitro drug release assay, to assess whether the NPs could sustain DFO release in a continuous manner. Briefly, a certain amount of DFO-loaded NPs were dissolved in 5 mL of phosphate buffered saline (PBS) to make a homogeneous solution, then transferred into a dialysis bag made of regenerated cellulose membranes (Spectrum, Houston, TX, USA). Afterwards, the bag was placed into a centrifuge tube with 15 mL of PBS as release medium. The tube was allowed to incubate at 37 °C whilst shaking at 120 rpm during the time range of this release study. Aliquot PBS dialysate was removed and replaced at predetermined time points and frozen until analyses. Before using HPLC to determine released DFO content, all samples were filtrated through Durapore PVDF filters (pore size of 0.45 μm; Millipore, Ireland), with 4 mM of $FeCl_3$ (Sigma-Aldrich) mixed in the same volume. The mobile phase here was prepared with acetonitrile: PBS ratio at (10%:90% v/v), adding 20 mM of ethylenediaminetetraacetic acid (EDTA), and the UV detection was carried out at λ_{max} of 440 nm under adjusted PH of 6.5 [41]. The release assay was performed thrice to obtain validated HPLC results, according to a calibration curve.

4.6. Cell Culture

The use of hBMSCs and HUVECs in the present study was approved by the ethical committee of Shanghai Sixth People's Hospital, with written informed consents of the donors. hBMSCs were isolated and cultured using standard protocols [44]. Briefly, bone marrow of femora midshaft was aspirated and suspended in T75 tissue culture flasks (Sarstedt, Ireland) in alpha-minimum essential medium (α-MEM; Gibco, Invitrogen Pty Ltd., Thornton, Australia), supplemented with 10% fetal bovine serum (FBS; Gibco) and 50 U/mL penicillin/streptomycin (Sigma-Aldrich), and cultured at 37 °C in a 5% CO_2 humidified atmosphere. The medium were changed every 3 days with non-adherent cells discarded, and the living cells were trypsinized and passaged at a ratio of 1:3 upon reaching 80% confluency. Cells of passage P3–5 were used for the following experiments. HUVECs were isolated from the human umbilical cord vein as previously described [45]. Cell pellets were resuspended in

Dulbecco's modified Eagle's medium (DMEM; Gibco) supplemented with 10% FBS and 1% endothelial cell growth supplement (ECGS/H, Promocell, Heidelberg, Germany).

4.7. In Vitro Cell Viability Assessment

The cytotoxicity of the blank and DFO-loaded NPs were evaluated by the conventional CCK-8 (Dojindo, Kumamoto, Japan) assay. Briefly, hBMSCs were seeded on 24-well plate (Corning, Inc., Corning, NY, USA) at a density of 1×10^4 cells/well, allowed to adhere overnight, and then solutions of blank NPs or DFO-loaded NPs were added. After incubating for 24, 48, and 72 h, the medium was removed and 100 μL of medium containing CCK-8 was added. Following incubation for another 2 h, the absorbance of the medium was measured using a spectrophotometer (Bio-Rad, Hercules, CA, USA) at 450 nm. The experiment was replicated for 3 times independently of each group.

A Live/Dead cell staining (ScienCell, Carlsbad, CA, USA) assay was also performed to estimate the cell death ratio, which could serve as an indication of NPs or DFO toxicity. In brief, after 72 h of incubation, the Live/Dead cell staining solution was added to each well and incubated for a further 30 min, then images were captured from 6 randomly chosen fields of each sample using a fluorescence microscope and cell number was counted. Live cells were green with green-fluorescent calcein-AM and dead cells were stained red with red-fluorescent ethidium homodimer-1.

4.8. Enzyme-Linked Immunosorbent Assay

Enzyme-linked immunosorbent assay (ELISA) was used to evaluate protein secretion levels of VEGF, bFGF and TGF-β1 from hBMSCs treated with or without the NPs. Briefly, cells were seeded on 24-well plate at a density of 1×10^4 cells/well. After exposing to the experimental conditions (blank or DFO-loaded NPs solution) for 48 h, protein levels of corresponding group were measured by ELISA (R&D Systems, Minneapolis, MN, USA). Notably, acidification of the supernatant media was applied before the ELISA assessment for TGF-β1 [46,47]. All experiments were repeated for three times.

4.9. Western Blot Analysis

For the Western blot assay, hBMSCs were cultured on 6-well plate (at a density of 1×10^5 cells/well), with either blank or DFO-loaded NPs dissolved in the medium. After culturing for 3 days, cells were collected and lysed to extract total cellular proteins. Next, the protein concentrations were quantified by a BCA protein assay kit (Beyotime, Nantong, China). Then, each protein sample weighing 40 μg was separated by sodium dodecyl sulfate-polyacrylamide gel electrophoresis (SDS-PAGE) and transferred to polyvinylidene difluoride (PVDF) membranes. After blocked with bovine serum albumin (BSA) for 1 h, the membranes were incubated with primary antibody of anti-HIF-1α (1:500; Abcam, City, UK), and detected using a horseradish peroxidase (HPR)-conjugated secondary antibody (1:5000; Sigma, Santa Clara, CA, USA). β-actin antibody (1:2000) was used for normalization of protein loading. The HIF-1α protein was visualized using the Enhanced Chemiluminescence System (Cell Signaling Technology Inc., Boston, MA, USA).

4.10. ALP Activity Evaluation

hBMSCs were seeded on 24-well plates at the density of 1×10^5 cells/well. After cells reached confluence, the culture medium was replaced by osteogenic differentiation medium, consisting of 0.15 mM ascorbate-2-phosphate, 2 mM β-glycerophosphate and 10^{-7} M dexamethasone (Sigma-Aldrich). The blank or DFO-loaded NPs were then added. Cells were incubated for 7 and 14 days before the following evaluation. According to the manufacturer's instructions, cells were firstly washed with PBS for 3 times and with cold 50 mM Tris buffer once, respectively. Secondly, 200 μL of 0.2% Triton X-100 was pipetted in to lyse the cells. Next, the lysates were centrifuged at 14,000 rpm for 15 min and sonicated. Then, a volume of 150 μL working solution was mixed with 50 μL of the aforementioned supernatant, and the conversion of *p*-nitrophenyl phosphate into *p*-nitrophenol

mediated by ALP was assessed by measuring the absorbance at 405 nm with a microplate reader (Bio-Rad 680, Hercules, CA, USA).

4.11. Angiogenic and Osteogenic mRNA Expressions of DFO-Loaded PLGA-PEG-PLGA NPs-Treated hBMSCs

The qRT-PCR was performed to evaluate the effects of the released DFO on angiogenic and osteogenic differentiation gene expressions in hBMSCs. Before examining angiogenic-related gene expressions, hBMSCs were cultured for 12 or 48 h in control medium (α-MEM supplemented with 10% FBS) containing blank or DFO-loaded NPs. Meanwhile, to monitor the expression alterations of osteogenic differentiation genes, hBMSCs were cultured in osteogenic differentiation medium mentioned above with NPs added. After incubating for 7 days, 1 mL of Trizol (Invitrogen, Carlsbad, CA, USA) was added, incubated overnight at 4 °C to extract total cytoplasmic RNA. Then, cDNA was synthesized using 1 μg of RNA and PrimeScript First Strand cDNA Synthesis Kit (Takara, Japan). Finally, gene expression was evaluated by qRT-PCR using a SYBR Green qPCR kit (Takara) in combination with ABI 7500 Real-Time PCR System (Applied Biosystems, Waltham, MA, USA). The relative levels of the mRNA was normalized to that of endogenous reference gene glyceraldehyde-3-phosphate dehydrogenase (GAPDH). The primers were synthesized as follows: VEGF: forward, 5′-GCACCCATGGCAGAAGGAGG-3′, and reverse, 5′-CCTTGGTGAGG TTTGATCCGCATA-3′; bFGF: forward, 5′-GGAGAAGAGCGACCCTCACATCAAG-3′, and reverse, 5′-CCAGTTCGTTTCAGTGCCACATACCAA-3′; TGF-β1: forward, 5′-GGTCACCCGCG TGCTAATGG-3′, and reverse, 5′-GTGGAGCTGAAGCAATAGTTGG-3′; Osteocalcin: forward, 5′-GGCGCTACCTGTATCAATGG-3′, and reverse, 5′-TCAGCCAACTCGTCACAGTC-3′; Runx-2: forward, 5′-CAAAGGTGCAGCCTTTGTGTC-3′, and reverse, 5′-TCACAGTCCGGATTGAGCTCA-3′; GAPDH: forward, 5′-CGGATTTGGTCGTATTGGGC-3′, and reverse, 5′-GTCATACCAGGAAATGAGCTTG-3′.

4.12. Evalution of the Angiogenic Effect of DFO-Loaded PLGA-PEG-PLGA NPs on HUVECs

Briefly, HUVECs were cultured on the lower chamber of 6-well transwell plate at a density of 1×10^5 cells/well, and DFO-loaded NPs solution of 1 mL was added into the upper chamber. After pipetting 3 mL of DMEM (Gibco) into the lower chamber, the upper inserts were placed in wells and hanging above the HUVECs monolayer. It is envisaged that DFO released from the NPs was able to diffuse through the insert membrane (5 μm of pore size; Millipore, County Cork, Ireland) towards the HUVECs culture medium, and exerted effect on the cell monolayer. Meanwhile, wells without inserts, or inserts containing blank NPs were used as control. qRT-PCR was used to evaluate the transcript expression of VEGF, ANGPT-2, EGF and PDGF-BB at 24, 48 and 72 h, performed in procedures as mentioned above. The primers were synthesized as follows: VEGF: forward, 5′-CTACCTCCACCATGCCAAGT-3′, and reverse, 5′-ATGTTGGACTCCTCAGTGGG-3′; ANGPT-2: forward, 5′-GGATGGAGACAACGACAAATG-3′, and reverse, 5′-GGACCACAT GCATCAAACC-3′; EGF: forward, 5′-AAGAATGGGGGTCAACCAGT-3′, and reverse, 5′-TGAAGTTGGTTGCATTGACC-3′; PDGF-BB: forward, 5′-CTGGCATGCAAGTGTGAGAC-3′, and reverse, 5′-CGAATGGTCACCCGAGTTT-3′; GAPDH: forward, 5′-GTCAGTGGTGGACCTGACCT-3′, and reverse, 5′-AGGGGTCTACATGGCAACTG-3′.

Afterwards, we investigated the tube formation activity of the HUVECs in the existence of DFO-loaded NPs. Briefly, 500 μL of thawed Matrigel (BD Bioscience, San Jose, CA, USA) was transferred onto 24-well plate and incubated at 37 °C for solidification. Then, the solidified Matrigel was overlaid with HUVECs which had been starved in serum-free medium for 24 h, at a density of 3×10^4 cells/well. Next, the blank or DFO-loaded NPs were placed into the wells. Microscopic images were taken from 5 randomly chosen fields of each sample 24 h later, and the tube formation activity was determined by calculating the number of complete capillaries which connected individual points of the polygonal frameworks.

4.13. Statistical Analysis

All data were expressed as mean ± standard deviation (SD). For comparisons between two groups, the data were analyzed with a Student's *t*-test to determine the level of significance, and $p < 0.05$ were considered statistically significant. Statistical analyses were performed using the SPSS 10.0 statistical software (SPSS, Chicago, IL, USA).

5. Conclusions

In this study, we successfully prepared PLGA-PEG-PLGA triblock copolymers and PLGA-PEG-PLGA NPs through ring-opening polymerization and a modified solvent extraction/evaporation method, respectively. On the one hand, the PLGA-PEG-PLGA NPs have excellent physical and chemical properties for biological use; on the other hand, this NPs system could act as an efficient drug delivery vehicle for DFO with reasonable biocompatibility. Additionally, systematic in vitro experiments demonstrated that the angiogenic and osteogenic effects of the released DFO on hBMSCs and HUVECs were well preserved over a long time course. Taken together, this novel DFO-loaded PLGA-PEG-PLGA NPs may possibly be used as a therapeutic strategy in the management of bone defects in the future.

Acknowledgments: This work was supported by the National High-Tech Research and development program (863-Project, No. 2015AA020316).

Author Contributions: Manle Qiu and Yaohua He conceived and designed the experiments; Manle Qiu and Chongyang Wang performed the experiments, Daoyun Chen and Huakun Zhao acquired and analyzed the data; Manle Qiu drafted the manuscript; Chaoyong Shen helped perform the analysis with constructive discussions and revised the manuscript.

Conflicts of Interest: The authors declare no conflict of interest.

References

1. Min, Z.; Shichang, Z.; Chen, X.; Yufang, Z.; Changqing, Z. 3D-printed dimethyloxallyl glycine delivery scaffolds to improve angiogenesis and osteogenesis. *Biomater. Sci.* **2015**, *3*, 1236–1244. [CrossRef] [PubMed]
2. Hankenson, K.D.; Dishowitz, M.; Gray, C.; Schenker, M. Angiogenesis in bone regeneration. *Injury* **2011**, *42*, 556–561. [CrossRef] [PubMed]
3. Weiss, S.; Zimmermann, G.; Pufe, T.; Varoga, D.; Henle, P. The systemic angiogenic response during bone healing. *Arch. Orthop. Trauma Surg.* **2009**, *129*, 989–997. [CrossRef] [PubMed]
4. Potier, E.; Ferreira, E.; Dennler, S.; Mauviel, A.; Oudina, K.; Logeart-Avramoglou, D.; Petite, H. Desferrioxamine-driven upregulation of angiogenic factor expression by human bone marrow stromal cells. *J. Tissue Eng. Regen. Med.* **2008**, *2*, 272–278. [CrossRef] [PubMed]
5. Quarto, R.; Mastrogiacomo, M.; Cancedda, R.; Kutepov, S.M.; Mukhachev, V.; Lavroukov, A.; Marcacci, M. Repair of large bone defects with the use of autologous bone marrow stromal cells. *N. Engl. J. Med.* **2001**, *344*, 385–386. [CrossRef] [PubMed]
6. Cancedda, R.; Bianchi, G.; Derubeis, A.; Quarto, R. Cell therapy for bone disease: A review of current status. *Stem Cells* **2003**, *21*, 610–619. [CrossRef] [PubMed]
7. Petite, H.; Viateau, V.; Bensaid, W.; Meunier, A.; de Pollak, C.; Bourguignon, M.; Guillemin, G. Tissue-engineered bone regeneration. *Nat. Biotechnol.* **2000**, *18*, 959–963. [CrossRef] [PubMed]
8. Zhang, J.; Guan, J.; Qi, X.; Ding, H.; Yuan, H.; Xie, Z.; Huang, Y. Dimethyloxaloylglycine Promotes the Angiogenic Activity of Mesenchymal Stem Cells Derived from iPSCs via Activation of the PI3K/Akt Pathway for Bone Regeneration. *Int. J. Biol. Sci.* **2016**, *12*, 639–652. [CrossRef] [PubMed]
9. Wang, Y.; Wan, C.; Gilbert, S.R.; Clemens, T.L. Oxygen sensing and osteogenesis. *Ann. N. Y. Acad. Sci.* **2007**, *1117*, 1–11. [CrossRef] [PubMed]
10. Saito, T.; Tabata, Y. Hypoxia-induced angiogenesis is increased by the controlled release of deferoxiamine from gelatin hydrogels. *Acta Biomater.* **2014**, *10*, 3641–3649. [CrossRef] [PubMed]
11. Jaakkola, P.; Mole, D.R.; Tian, Y.M.; Wilson, M.I.; Gielbert, J.; Gaskell, S.J.; Maxwell, P.H. Targeting of HIF-α to the von Hippel-Lindau ubiquitylation complex by O_2-regulated prolyl hydroxylation. *Science* **2001**, *292*, 468–472. [CrossRef] [PubMed]

12. Min, J.H.; Yang, H.; Ivan, M.; Gertler, F.; Kaelin, W.G.; Pavletich, N.P. Structure of an HIF-1α-pVHL complex: Hydroxyproline recognition in signaling. *Science* **2002**, *296*, 1886–1889. [CrossRef] [PubMed]
13. Kontoghiorghes, G.J.; Spyrou, A.; Kolnagou, A. Iron chelation therapy in hereditary hemochromatosis and thalassemia intermedia: Regulatory and non regulatory mechanisms of increased iron absorption. *Hemoglobin* **2010**, *34*, 251–264. [CrossRef] [PubMed]
14. Chung, J.H.; Kim, Y.S.; Noh, K.; Lee, Y.M.; Chang, S.W.; Kim, E.C. Deferoxamine promotes osteoblastic differentiation in human periodontal ligament cells via the nuclear factor erythroid 2-related factor-mediated antioxidant signaling pathway. *J. Periodontal Res.* **2014**, *49*, 563–573. [CrossRef] [PubMed]
15. Jia, P.; Chen, H.; Kang, H.; Qi, J.; Zhao, P.; Jiang, M.; Guo, L.; Zhou, Q.; Qian, N.D.; Zhou, H.B.; et al. Deferoxamine released from poly (lactic-co-glycolic acid) promotes healing of osteoporotic bone defect via enhanced angiogenesis and osteogenesis. *J. Biomed. Mater. Res. A* **2016**, *104*, 2515–2527. [CrossRef] [PubMed]
16. Hallaway, P.E.; Eaton, J.W.; Panter, S.S.; Hedlund, B.E. Modulation of deferoxamine toxicity and clearance by covalent attachment to biocompatible polymers. *Proc. Natl. Acad. Sci. USA* **1989**, *86*, 10108–10112. [CrossRef] [PubMed]
17. Ikeda, Y.; Tajima, S.; Yoshida, S.; Yamano, N.; Kihira, Y.; Ishizawa, K.; Tamaki, T. Deferoxamine promotes angiogenesis via the activation of vascular endothelial cell function. *Atherosclerosis* **2011**, *215*, 339–347. [CrossRef] [PubMed]
18. Pham, H.; Nguyen, Q.P. Effect of silica nanoparticles on clay swelling and aqueous stability of nanoparticle dispersions. *J. Nanopart. Res.* **2014**, *16*, 1–11. [CrossRef] [PubMed]
19. Wang, T.; Zhu, D.; Liu, G.; Tao, W.; Cao, W.; Zhang, L.; Zeng, X. DTX-loaded star-shaped TAPP-PLA-b-TPGS nanoparticles for cancer chemical and photodynamic combination therapy. *RSC Adv.* **2015**, *5*, 50617–50627. [CrossRef]
20. Liao, S.H.; Liu, C.H.; Bastakoti, B.P.; Suzuki, N.; Chang, Y.; Yamauchi, Y.; Wu, K.C. Functionalized magnetic iron oxide/alginate core-shell nanoparticles for targeting hyperthermia. *Int. J. Nanomed.* **2015**, *10*, 3315–3328.
21. Suárez-González, D.; Barnhart, K.; Saito, E.; Vanderby, R.; Hollister, S.J.; Murphy, W.L. Controlled nucleation of hydroxyapatite on alginate scaffolds for stem cell-based bone tissue engineering. *J. Biomed. Mater. Res. A* **2010**, *95*, 222–234.
22. Lin, H.R.; Yeh, Y.J. Porous alginate/hydroxyapatite composite scaffolds for bone tissue engineering: Preparation, characterization, and in vitro studies. *J. Biomed. Mater. Res. B Appl. Biomater.* **2004**, *71*, 52–65. [CrossRef] [PubMed]
23. Tomasina, J.; Lheureux, S.; Gauduchon, P.; Rault, S.; Malzert-Fréon, A. Nanocarriers for the targeted treatment of ovarian cancers. *Biomaterials* **2013**, *34*, 1073–1101. [CrossRef] [PubMed]
24. Liang, Y.H.; Liu, C.H.; Liao, S.H.; Lin, Y.Y.; Tang, H.W.; Liu, S.Y.; Wu, K.C.W. Cosynthesis of cargo-loaded hydroxyapatite/alginate core–shell nanoparticles (HAP@ Alg) as pH-responsive nanovehicles by a pre-gel method. *ACS Appl. Mater. Interfaces* **2012**, *4*, 6720–6727. [CrossRef] [PubMed]
25. Gao, N.; Chen, Z.; Xiao, X.; Ruan, C.; Mei, L.; Liu, Z.; Zeng, X. Surface modification of paclitaxel-loaded tri-block copolymer PLGA-b-PEG-b-PLGA nanoparticles with protamine for liver cancer therapy. *J. Nanopart. Res.* **2015**, *17*, 1–11. [CrossRef]
26. Yu, L.; Zhang, H.; Ding, J. Effects of precipitate agents on temperature-responsive sol–gel transitions of PLGA–PEG–PLGA copolymers in water. *Colloid Polym. Sci.* **2010**, *288*, 1151–1159. [CrossRef]
27. Long, F. Building strong bones: Molecular regulation of the osteoblast lineage. *Nat. Rev. Mol. Cell Biol.* **2012**, *13*, 27–38. [CrossRef] [PubMed]
28. Saran, U.; Piperni, S.G.; Chatterjee, S. Role of angiogenesis in bone repair. *Arch. Biochem. Biophys.* **2014**, *561*, 109–117. [CrossRef] [PubMed]
29. Mayr-Wohlfart, U.; Waltenberger, J.; Hausser, H.; Kessler, S.; Günther, K.P.; Dehio, C.; Brenner, R.E. Vascular endothelial growth factor stimulates chemotactic migration of primary human osteoblasts. *Bone* **2002**, *30*, 472–477. [CrossRef]
30. Deckers, M.M.; Karperien, M.; van der Bent, C.; Yamashita, T.; Papapoulos, S.E.; Löwik, C.W. Expression of vascular endothelial growth factors and their receptors during osteoblast differentiation. *Endocrinology* **2000**, *141*, 1667–1674. [CrossRef] [PubMed]
31. Wang, Y.; Wan, C.; Deng, L.; Liu, X.; Cao, X.; Gilbert, S.R.; Haase, V.H. The hypoxia-inducible factor α pathway couples angiogenesis to osteogenesis during skeletal development. *J. Clin. Investig.* **2007**, *117*, 1616–1626. [CrossRef] [PubMed]

32. Weinreb, O.; Amit, T.; Mandel, S.; Youdim, M.B. Novel therapeutic approach for neurodegenerative pathologies: Multitarget iron-chelating drugs regulating hypoxia-inducible factor 1 signal transduction pathway. *Neurodegener. Dis.* **2011**, *10*, 112–115. [CrossRef] [PubMed]
33. Xiao, J.; Lv, Y.; Lin, B.; Tipoe, G.L.; Youdim, M.B.; Xing, F.; Liu, Y. A Novel Antioxidant Multitarget Iron Chelator M30 Protects Hepatocytes against Ethanol-Induced Injury. *Oxid. Med. Cell. Longev.* **2015**, *2015*, 607271. [CrossRef] [PubMed]
34. Golko-Perez, S.; Amit, T.; Youdim, M.B.; Weinreb, O. Beneficial Effects of Multitarget Iron Chelator on Central Nervous System and Gastrocnemius Muscle in SOD1G93A Transgenic ALS Mice. *J. Mol. Neurosci.* **2016**, 1–7. [CrossRef] [PubMed]
35. Kim, M.K.; Park, H.J.; Kim, Y.D.; Ryu, M.H.; Takata, T.; Bae, S.K.; Bae, M.K. Hinokitiol increases the angiogenic potential of dental pulp cells through ERK and p38MAPK activation and hypoxia-inducible factor-1α (HIF-1α) upregulation. *Arch. Oral. Biol.* **2014**, *59*, 102–110. [CrossRef] [PubMed]
36. Fox, M.E.; Szoka, F.C.; Fréchet, J.M. Soluble polymer carriers for the treatment of cancer: The importance of molecular architecture. *Acc. Chem. Res.* **2009**, *42*, 1141–1151. [CrossRef] [PubMed]
37. Mei, L.; Zhang, Y.; Zheng, Y.; Tian, G.; Song, C.; Yang, D.; Li, Z. A novel docetaxel-loaded poly (ε-caprolactone)/pluronic F68 nanoparticle overcoming multidrug resistance for breast cancer treatment. *Nanoscale Res. Lett.* **2009**, *4*, 1530–1539. [CrossRef] [PubMed]
38. Phromviyo, N.; Swatsitang, E.; Chompoosor, A. Effect of a surface stabilizer on the formation of polyoxalate nanoparticles and their release profiles. *Vacuum* **2014**, *107*, 208–212. [CrossRef]
39. Yu, J.; Li, X.; Luo, Y.; Lu, W.; Huang, J.; Liu, S. Poly (ethylene glycol) shell-sheddable magnetic nanomicelle as the carrier of doxorubicin with enhanced cellular uptake. *Colloids Surf. B Biointerfaces* **2013**, *107*, 213–219. [CrossRef] [PubMed]
40. Liang, H.F.; Chen, C.T.; Chen, S.C.; Kulkarni, A.R.; Chiu, Y.L.; Chen, M.C.; Sung, H.W. Paclitaxel-loaded poly (γ-glutamic acid)-poly (lactide) nanoparticles as a targeted drug delivery system for the treatment of liver cancer. *Biomaterials* **2006**, *27*, 2051–2059. [CrossRef] [PubMed]
41. Hastings, C.L.; Kelly, H.M.; Murphy, M.J.; Barry, F.P.; O'Brien, F.J.; Duffy, G.P. Development of a thermoresponsive chitosan gel combined with human mesenchymal stem cells and desferrioxamine as a multimodal pro-angiogenic therapeutic for the treatment of critical limb ischaemia. *J. Control. Release* **2012**, *161*, 73–80. [CrossRef] [PubMed]
42. Chekanov, V.S.; Zargarian, M.; Baibekov, I.; Karakozov, P.; Tchekanov, G.; Hare, J.; Akhtar, M. Deferoxamine-fibrin accelerates angiogenesis in a rabbit model of peripheral ischemia. *Vasc. Med.* **2003**, *8*, 157–162. [CrossRef] [PubMed]
43. Jiang, T.; Li, Y.; Lv, Y.; Cheng, Y.; He, F.; Zhuo, R. Biodegradable amphiphilic block-graft copolymers based on methoxy poly (ethylene glycol)-b-(polycarbonates-g-polycarbonates) for controlled release of doxorubicin. *J. Mater. Sci. Mater. Med.* **2014**, *25*, 131–139. [CrossRef] [PubMed]
44. Duffy, G.P.; Ahsan, T.; O'Brien, T.; Barry, F.; Nerem, R.M. Bone marrow–derived mesenchymal stem cells promote angiogenic processes in a time-and dose-dependent manner in vitro. *Tissue Eng. Part A* **2009**, *15*, 2459–2470. [CrossRef] [PubMed]
45. Barbucci, R.; Lamponi, S.; Magnani, A.; Piras, F.M.; Rossi, A.; Weber, E. Role of the Hyal-Cu (II) complex on bovine aortic and lymphatic endothelial cells behavior on microstructured surfaces. *Biomacromolecules* **2005**, *6*, 212–219. [CrossRef] [PubMed]
46. van Waarde, M.A.W.H.; van Assen, A.J.; Kampinga, H.H.; Konings, A.W.T.; Vujaskovic, Z. Quantification of Transforming Growth Factor-β in Biological Material Using Cells Transfected with a Plasminogen Activator Inhibitor-1 Promoter–Luciferase Construct. *Anal. Biochem.* **1997**, *247*, 45–51. [CrossRef] [PubMed]
47. Maire, M.; Logeart-Avramoglou, D.; Degat, M.C.; Chaubet, F. Retention of transforming growth factor β1 using functionalized dextran-based hydrogels. *Biomaterials* **2005**, *26*, 1771–1780. [CrossRef] [PubMed]

© 2016 by the authors; licensee MDPI, Basel, Switzerland. This article is an open access article distributed under the terms and conditions of the Creative Commons Attribution (CC-BY) license (http://creativecommons.org/licenses/by/4.0/).